24th Electromagnetic Induction Workshop

13-20 August 2018, Helsingør Denmark

www.emiw2018.org

Abstracts Session 6

SESSIONS DESCRIPTION

Session 6. Rock and Mineral Resistivity, and Anisotropy

The link between electrical resistivity from the laboratory/outcrop scale to lithospheric-asthenospheric scale is challenging due to several factors (sampling procedure, local heterogeneity, anisotropy on multiple scales, geological structure, coupling between rocks and fluids). Despite major experimental, theoretical and modelling advances a remaining future goal is the development of meaningful experiments and models that allow us to identify and quantify the relationship between causative processes and electrical rock resistivity on different scales and in different environments (P,T, fluids). This is a critical step in order to unravel the complex evolution and dynamics of the earth's lithosphere-asthenosphere and also to develop predictive capabilities for energy applications. In this session, we therefore welcome studies that adopt novel approaches and combined methodologies using experimental and numerical methods in the laboratory and the field related to rock and mineral resistivity, as well as developments in the study of electrical anisotropy.

Conveners: Jana Boerner, Juanjo Ledo, Ute Weckmann

Detectability of the resistivity anisotropy using the CSRMT method with a horizontal electric dipole

A. Shlykov[1], A. Saraev[2]
[1]St. Petersburg State University, Russia, shlykovarseny@gmail.com
[2]St. Petersburg State University, Russia, asaraev51@mail.ru

SUMMARY

The resistivity anisotropy is an important parameter for interpretation of electromagnetic soundings data. The importance of anisotropy was demonstrated by the marine electromagnetic community. Significant anisotropy is also observed in near surface media. In this abstracts we are discussing the detectability of anisotropy using land-based controlled source radiomagnetotellurics with a horizontal electric dipole. Our field experiment was performed in an area with 1D geology and two layers with strong a priori detected anisotropy. We are comparing controlled source high frequency responses in different geometries (inline and broadside), and the dependency of anisotropy detectability taking into account a length of the source using both numerical simulation and anisotropic inversion of field data.

Keywords: Anisotropy, Controlled-source radiomagnetotellurics, Transition zone, Horizontal electric dipole.

Introduction

The anisotropy of electrical resistivity is an important parameter for the correct interpretation of electromagnetic soundings data. The importance of anisotropy accounting was demonstrated using field data by the marine electromagnetic community. Marine sediments are usually anisotropic because of differing lithology and hydrocarbon reservoirs also exhibit significant anisotropy (Constable, 2010). The accounting of anisotropy is used for the correct interpretation of marine CSEM data. Also, the vertical resistivity helps to locate the reservoirs more confidently.

In near surface land-based exploration the anisotropic objects are also not exotic. For example, glacial sediments contain thin and electrically contrast layers of sand and clay. Existing experience in studying of the anisotropy for the solution of near surface tasks is limited and mostly based on modelling only (Christensen, 2000; Ivanov et al., 2011). Using of the traditional isotropic inversion of direct current (DC) data such as the electrical resistivity tomography (ERT) in significantly anisotropic media can lead to wrong results. It is known that in DC case an anisotropic layer has simple relations with its isotropic equivalent, and determined thickness *h* is significantly overestimated (Maillet, 1947):

$$\rho_{DC} = \sqrt{\rho_v \rho_h}, \qquad h_{DC} = \sqrt{\rho_v / \rho_h} \cdot h = \lambda \cdot h$$

Here ρ_h – horizontal resistivity, ρ_v – vertical resistivity, λ - coefficient of anisotropy.

The idea of estimation of the anisotropy in land-based survey is based on the joint inversion of DC soundings data and transient electromagnetic data (TEM). The main problem of this approach is the necessity to use two different methods.

The controlled-source radiomagnetotlluric method (CSRMT) is a near surface electromagnetic frequency domain soundings based on measuring the EM field of a vertical loop (Bastani, 2001) or a grounded cable (Saraev et al., 2017) in frequency range 1-1000 kHz. In the urban regions upper frequencies 10-1000 kHz can be covered by broadcast VLF-LF radio transmitters.

In this abstract we are discussing results of a field experiment for the estimation of anisotropy using data of the CSRMT method in the transition zone of the horizontal electric dipole (grounded cable). We are demonstrating the dependency of detectability of anisotropy for the relative source-receiver geometry and length of the source. Also, we are comparing obtained results with the theoretical sensitivity and a priori borehole and hydrogeological data.

Geology of the experimental area

The survey area is located near St. Petersburg, Russia. It is well studied and has horizontally layered structure. In this area the geological section contains following formations (from top to bottom):

1. Quaternary moraine loams (6-10 m);
2. Ordovician clayey limestones (11-13 m);
3. Ordovician shales (1 m).
4. Ordovician-Cambrian sandstones (10-15 m);
5. Cambrian blue clays (more than 150 m).

The layer of Cambrian clays (basement in our case) is highly anisotropic. Photos of clay samples are presented in Figure 1. It is easy to see many thin sand lenses in the clayey matrix with thicknesses about 1 cm and less. Hydrogeological researches show that the ratio of horizontal and vertical components of the molecular diffusion coefficient for this clay is about 3-6. Ratio of horizontal and vertical filtration coefficients is about 5-15 (Pankina, 2010).

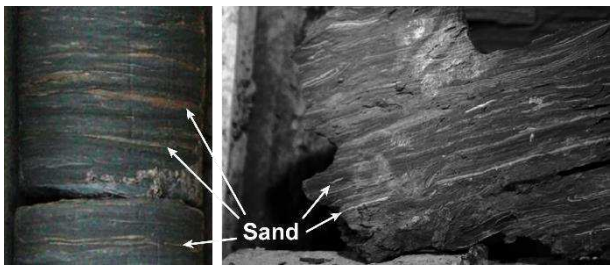

Figure 1. This lenses of sand in the Cambrian clays (Pankina, 2010).

The second anisotropic layer in the depth interval 10-35 m is a stack of limestones, shales and sands. Limestones contains alternation of thin more and less clayey sublayers. Between limestones and sandstones there is a thin layer of shales.

Field experiment

The field experiment using the CSRMT method for estimation of anisotropy was performed in two stages. The first stage was conducted in 2013 with relatively short (200 m length) grounded cable. Measurements were fulfilled along one profile using both inline and broadside geometries. Inline response was measured along the profile, broadside response - in perpendicular direction. The second stage of the field experiment was conducted in 2017 with the 500 m length grounded cable. In this case we used the broadside geometry only. Locations of profiles of measurements in 2013 and 2017 are not exactly the same but very close with deviation is about 10-20 m. The outline is presented in Figure 2.

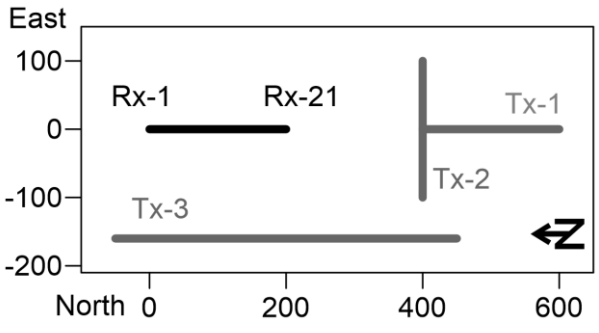

Figure 2. The outline of survey in different years.

I In all cases we have the strong transition field effect – significant impact of the galvanic mode of EM field. We will use following numbering: case 1 – inline geometry and 200 m length of the source, case 2 – broadside geometry and 200 m length of the source, case 3 – broadside geometry and 500 m length of the source. Inversion was performed using an 1D anisotropic code described in (Shlykov, Saraev, 2015). For the inversion we used scalar apparent resistivity and impedance phase along the corresponding source only. Figure 3 illustrates cross-section for obtained horizontal resistivity ρ_h, Figure 4 - for the coefficient of anisotropy λ.

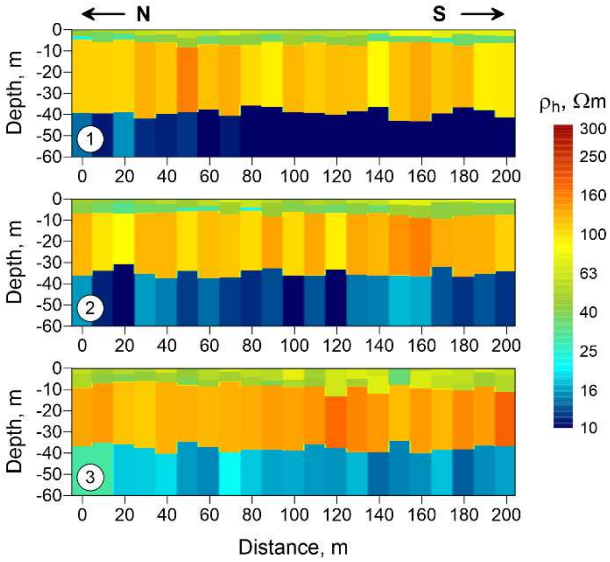

Figure 3. Cross-sections of horizontal resistivity for different source-receiver geometries.

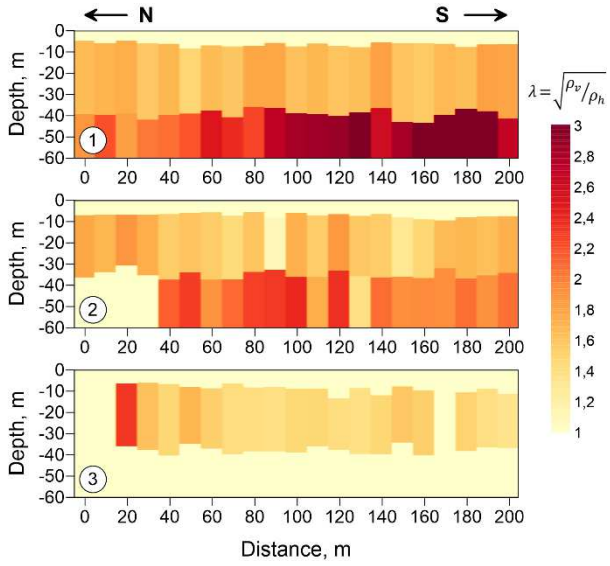

Figure 4. Cross-sections of anisotropy coefficient for different source-receiver geometries.

Four-layer structure is seen in Figure 3. Two upper layers are soil and moraine loams. The third layer is

stack of limestones, shales and sandstones. The fourth layer is represented by clays.

Top layers of soil and Quaternary moraine loams are resolved as isotropic because of no impact of galvanic mode at high frequencies (far-field zone). It has resistivity about 30-60 Ωm. The third resistive layer of limestones and sandstones is obviously anisotropic. In the first and second cases coefficient of anisotropy estimated by the inversion of CSRMT data was relatively similar, about 1.6-1.8. In the third case (broadside area of long source) λ = 1.3-1.6. In the area near to a grounding the coefficient of anisotropy was not resolved. In all cases the horizontal resistivity is near to 100 Ωm.

The bottom layer of clay is highly anisotropic. In the first case (inline measurements) λ = 1.8-3.0. The coefficient of anisotropy is decreased toward the North (Figure 4, 1). In this case the horizontal resistivity of clay is about 5-12 Ωm. In the second case the clays have λ = 1.9-2.3, but at the northern stations the coefficient of anisotropy was not resolved. Horizontal resistivity in this case is a little bit higher and varies from 9 to 17 Ωm. In the third case with long source the clays are shown as totally isotopic with horizontal resistivity near to 15-20 Ωm.

Modelling and discussion of results

Let's consider averaged 1D anisotropic model (Table 1) and integral sensitivity of apparent resistivity and impedance phase along the source for vertical resistivity of last two anisotropic layers.

Table 1. Averaged model for numerical simulation.

Layer's #	ρ_h, Ωm	ρ_v, Ωm	h, m
1	60	60	3
2	30	30	7
3	100	300	25
4	5	50	∞

Integral sensitivity has following expression [Zhdanov, 2002]:

$$S_{int} = \left\{ \sum_f \left[\frac{\partial ln(\rho_a)}{\partial ln(\rho_v)} \right]^2 + \sum_f \left[\frac{\partial ln(|\varphi_Z| + 45°)}{\partial ln(\rho_v)} \right]^2 \right\}^{\frac{1}{2}}$$

Here f – index of frequency. We use the transformation of ρ_a and φ_Z for making their dynamic range compatible. Integral sensitivity was calculated for three sources with lengths 200, 500 and 1000 m. Results are presented in Figures 5-6. Maps of the integral sensitivity explain all mismatches in the discussed results.

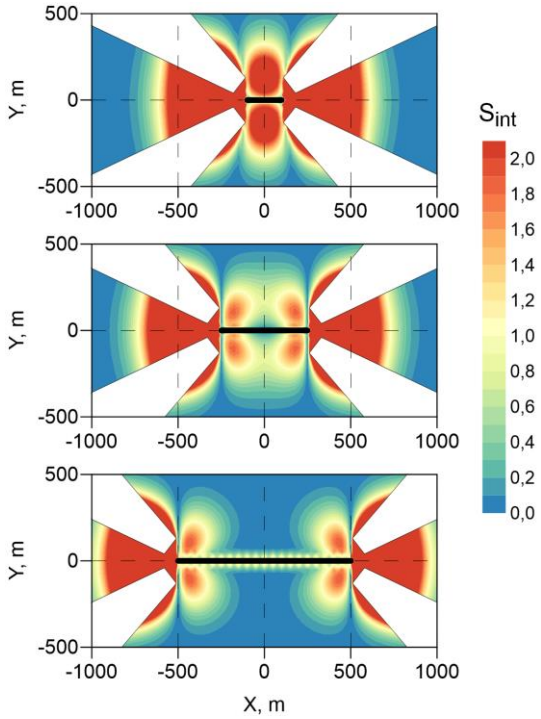

Figure 5. Integral sensitivity of Z_{xy} for vertical resistivity of third layer. Black solid line in the center is a source. White polygons mask areas of numerical instabilities because of structure of the normal field.

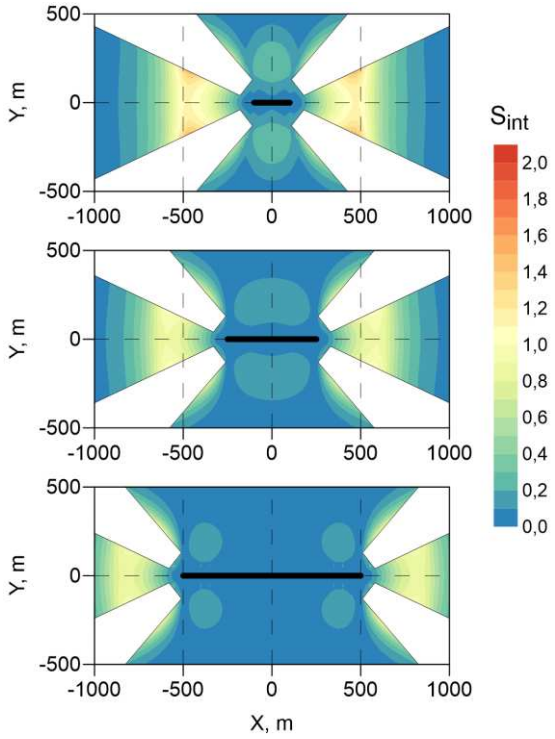

Figure 6. Integral sensitivity of Z_{xy} for vertical resistivity of fourth layer. Black solid line in the center is a source. White polygons mask areas of numerical instabilities because of structure of the normal field.

The inline data have the strongest sensitivity for ρ_v because of strong impact of the vertical electric field. It is also known from the marine CSEM (Constable, 2010). That is why the inline data show the most significant anisotropy including anisotropy of the conductive clays below the resistive and anisotropic limestones and sandstones. Moreover, the anisotropy of clays obtained from inline measurements is in good agreements with the hydrogeological data.

For our model the sensitivity to ρ_v in the broadside area of the long source is near to zero and is increased with decreasing of the length of source. It has simple physical explanation. In the near-field zone EM field is mostly galvanic and injected current goes sub vertically from groundings. In the broadside area the current is sub horizontal. When we use a short source the broadside response still contains the significant impact of vertical component of the electric field. That is why the anisotropy obtained with 500 m length of source is weaker. The anisotropy for broadside measurements with 200 m length of source is compatible with the inline results. Resistivity of clays in the third case is close to geometrical mean of ρ_h and ρ_v obtained by inline data according to the theoretical equivalency (Maillet, 1947).

The sensitivity has minimum in the area exactly in front of the grounding. That is why the anisotropy is totally unresolved in the third case near to the northern end of the profile.

Conclusions

Controlled source radiomagnetotellurics measurements in the transition zone of the grounded cable allow us to determine the anisotropy of resistivity. Detectability of the anisotropy is well controlled by the numerical simulations and theory. It is enough to use scalar impedance only for anisotropic inversion if the sensitivity is significant. Sensitivity to the vertical resistivity in the broadside area of the grounded cable depends on the length of the source and becomes zero with increasing of the length. Short source allows us to determine anisotropy in the broadside area even below the relatively resistive layer. Good agreement of results obtained in different years indicates the reliability of measurements. Anisotropy of the electrical resistivity obtained by CSRMT method is compatible with the hydrogeological data obtained in laboratory, but this relation have to be studied more carefully and is the subject of further research.

Acknowledgements

This study was supported by the Russian Foundation for Fundamental Researches, project No 17-55-45042, and the Center GEOMODEL of St. Petersburg State University.

References

Bastani M. (2001) EnviroMT – a new Controlled Source/Radio Magnetotelluric System. PhD thesis, Uppsala University, 179 p.

Constable S. (2010) Ten years of marine CSEM for hydrocarbon exploration. Geophysics, 75, pp. 67-81.

Christensen N.B. (2000) Difficulties in determining electrical anisotropy in subsurface investigations. Geophysical Prospecting, 48, pp. 1-19.

Ivanov P.V., Alexeev D.A., Bobachev A.A., Pushkarev P.J., Yacovlev A.G. (2011) About complexing the vertical electric soundings and near-field time domain electromagnetic. Engineer exploration, 11, pp. 42-51 (in Russian).

Maillet R. (1947) The fundamental equations of electrical prospecting. Geophysics, 12, pp. 529–556.

Pankina E.B., Ruminin V.G., Nikulenkov A.M., Glukhova M.P., Epimakhov V.N., Mysik S.G., Baev M.N., Kobekov V.V., Degtev V.F. (2010) Anisotropy of clays in diffusion transport of radionuclides. Radiochemistry, 52, pp. 630-637.

Saraev A., Simakov A., Shlykov A., Tezkan B. (2017) Controlled-source radiomagnetotellurics: A tool for near surface investigations in remote regions. Journal of App Geophys, 146, pp. 228-237.

Shlykov A.A., Saraev A.K. (2015) Estimation the macroanisotropy of a horizontally layered section from controlled-source radiomagnetotelluric soundings. Izvestiya, Physics of Solid Earth, Vol. 51, No. 4, pp. 583-601.

Zhdanov M.S., (2002) Geophysical inverse theory and regularization problems. (1st edn), Elsevier, USA, 633 p.

Electrical Properties of Carbonate Rocks
Insights from Multi-Method Laboratory Investigations

J.H. Börner[1], V. Herdegen[2], A. Rieger[2], J.-U. Repke[3] and K. Spitzer[1]
[1]Institute of Geophysics and Geoinformatics, Technical University Bergakademie Freiberg (Germany), jana.boerner@geophysik.tu-freiberg.de
[2]Institute of Thermal, Environmental and Natural Products Process Engineering, Technical University Bergakademie Freiberg (Germany)
[3]Institute of Process Technology and Process Engineering, Technical University Berlin (Germany)

SUMMARY

Carbonatic reservoirs have come into focus because they host huge resources of oil and natural gas. Consequently, they are also targets for enhanced oil recovery and CO_2 sequestration techniques. In this context, electromagnetic methods can be of great value because they are sensitive to the pore content and provide information on the electrical properties of large rock volumes. Nevertheless, the petrophysical knowledge of the electrical properties of carbonates, which is an essential basis of monitoring, is still rather crude.

This lack is due to the great challenges that carbonate rocks pose for petrophysics, exploration geophysics and reservoir engineering. The reactive nature of the carbonate minerals causes them to react by dissolution, precipitation and varying surface complexation to any change in pore filling or environmental conditions. This is complicated further by their varying genesis and geologic history resulting in

- a varying mineralogical composition,
- multiple types of pore space (intercrystalline, interparticle, oomoldic, vuggy),
- an extreme multi-scale heterogeneity of petrophysical properties.

The presence of a reactive gas such as CO_2, which is commonly used in enhanced oil recovery applications, causes additional interactions and has to be considered particularly during monitoring. We therefore systematically investigate the petrophysical properties of carbonate rocks under both normal and reservoir conditions in the laboratory with multiple petrophysical methods. We use both plugs and crushed samples of varying particle size. This approach reduces the complexity of the entire system and lets us differentiate between electro-chemical interaction and pore-space controlled processes.

We have investigated the particle shape and size, pore space (porosity, nuclear magnetic resonance, mercury intrusion porosimetry, microCT), surface properties (nitrogen adsorption), composition (chemical analyses, X-ray diffraction) and electrical properties (spectral induced polarization) on a set of plugs and 8 fractions of crushed samples, each from four carbonates and one sandstone (for comparison). We demonstrate the variable properties of carbonates despite very high contents of carbonate minerals for all rocks.

Based on information from nuclear magnetic resonance and mercury intrusion porosimetry, basic statements on pore body and pore throat diameters become possible, which are linked to the electrical properties. The spectral induced polarization shows a general tendency of low imaginary conductivity for either low surface area or particularly high carbonate mineral content reflecting the importance of both size and complexation of the fluid-rock interface.

Combining the findings of the different petrophysical methods allows for the deduction of a model conception for origin and dependences of electric conduction in carbonate rocks. We further aim at a systematic quantification of the relevant processes in terms of their electrical manifestation and the derivation of a model description. The combined approach of spectral induced polarization, nuclear magnetic resonance, mercury intrusion porosimetry and accompanying analyses allows for the assessment of monitoring options with electrical methods in carbonatic reservoirs.

Electrical resistivity imaging over a buried elongated dipping conductor using Dipole-dipole and quasi null configurations

Mohammad Zubair[1], Anita Devi[1], Mohammad Israil[1], Pravin K Gupta[1]
[1]Indian Institute of Technology, Roorkee, 247667, India, zubairmohammadiitr@gmail.com

SUMMARY

The effect of dipping and finite strike length of a dipping conductor has been evaluated through 2D inversion of the ERT data recorded over a special analogue modelling designed experiment. The experiment allows us to control model depth and dip and to create real field conditions. Beside of the traditional array (Dipole-dipole) for detecting horizontal resistivity changes, new designed electrodes configurations (Szalai et al., 2014a) referred as γ11n quasi null arrays, the γ112, γ114 and γ116 and γ qnull were also used for the field test measurements. To invert the data of newly designed electrode configuration 2D inversion code (Szalai et al., 2014a) has been used. From the measurements it has been found that in most studied situations independently from its dipping all studied arrays were able to detect the conductor (graphite rod) which was embedded in sand and the dipping did not seem to influence the results significantly. In case of the largest dipping (30°) however the γ11n arrays showed a clearer image of the conductor. The difference between the conventional array and newly designed arrays can be seen more clearly using γ114 and γ116 arrays - which are closer to the null arrays. Based on the present study it can be stated that newly designed arrays which are closer to the null array are more suitable to delineate the geometry of the subsurface conductor than the Dipole-dipole or the γ112 arrays. In large depth they were even the only arrays which could detect the model.

Keywords: Electrical Resistivity Tomography (ERT), null array, quasi null array, dipping model

INTRODUCTION

Electrical Resistivity Tomography (ERT) measurement uses the concept of standard four electrodes system (two electrodes for current injection referred as source and sink) and other two electrodes are used to measure potential difference between them. These four electrodes are place in a particular geometry according to the chosen electrodes configuration e. g. Schlumberger, Wenner, dipole-dipole etc. (Keller and Friscknecht 1966). Measured response in the form of apparent resistivity is derived by multiplying geometrical factor with the measured resistance for each data point. In ERT measurements large number of electrodes are deployed along predefined profile line with fixed inter-electrode spacing. All the electrodes are connected to the measuring system (resistivity meter) through multi-core cable. The measuring system automatically select particular set of four electrodes through software designed sequence, preloaded in the system, for each measurement. In addition to the traditional electrode configurations, some new electrodes arrays referred as null-, and quasi null arrays have been designed by Szalai et al. (2002), Falco et al. (2013), Szalai et al. (2014a). On the basis of numerical modeling experiments they have shown that the new arrays can produced better resolved model both in horizontal and vertical direction and they have larger Depth of Detectability than any traditional geoelectric arrays (Szalai et al. 2014b). In the present paper we compare the results of traditional and newly designed array over a conducting body.

DATA RECORDED OVER A FIELD DESIGNED EXPERIMENTAL SETUP

An artificial pit of dimension 2x2x0.5 m^3 was prepared in the ground of Earth Sciences department of the Indian Institute of Technology Roorkee. In order to prepare host medium homogeneous and isotropic, the pit was filled with sand. A graphite rod of 0.80 m length and cross section area of 0.05 m^2 is buried in the sand horizontally and with 3 different dipping. With the different dip, the rod reached the following depths: 0.10, 0.20 and 0.40 m. ERT profiles data were recorded perpendicular to the strike of graphite rod model (Figure 1). IRIS Syscal Junior multi-electrodes (48 electrodes) imaging system with inter-electrodes spacing of 0.05 m was used for measurements.

To compare performance of traditional and newly designed electrodes configurations, we recorded dipole-dipole (Dp) and three members of the series of the γ11n quasi null arrays, the γ112, γ114, γ116 and γqnull (Szalai et al. (2014a) data along three profiles. The electrodes geometry of applied arrays is presented in Figure 2. Dp array was used because it proved to produce the highest Depth of Detectability (Szalai et al. 2014b) and its imaging properties proved to be the better (Szalai et al. 2013) among the traditional arrays. Total number of

data points recorded for these arrays are: Dp: 906, γ112: 528, γ114: 336, γ116: 240, γqnull: 414.

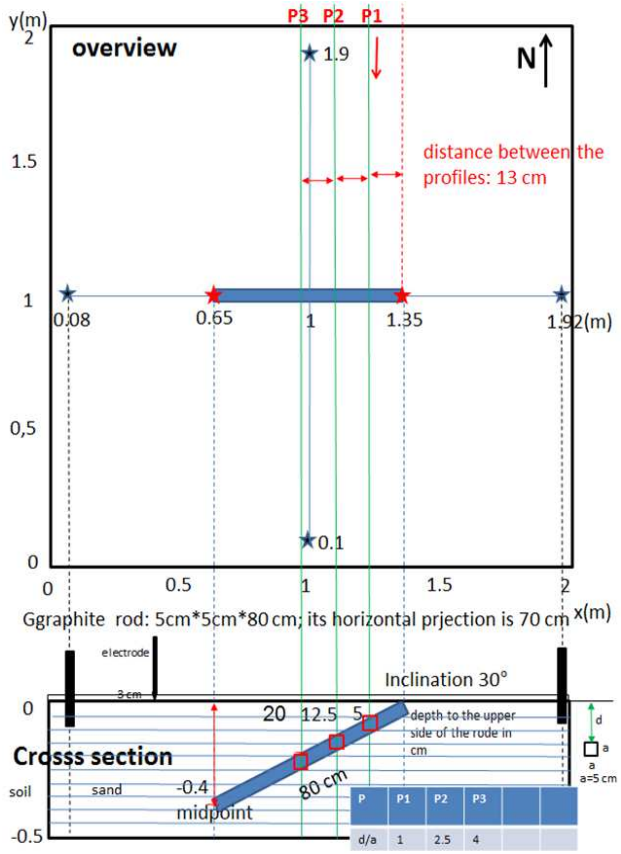

Figure 1: Geometry of buried conductor and profile lines for the situation with the largest dipping.

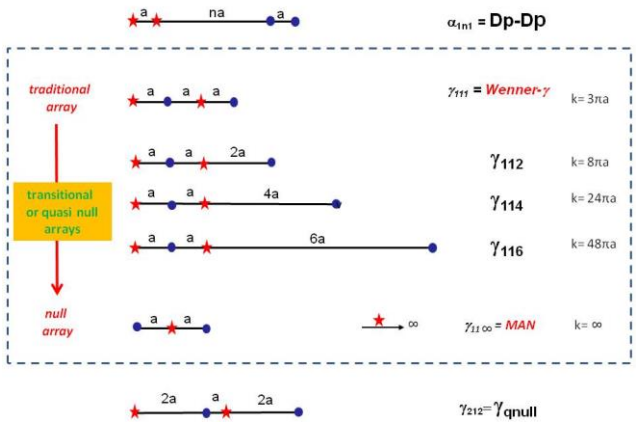

Figure 2: The applied geoelectric arrays. Stars: current electrodes. Filled circles: potential electrodes.

RESULTS AND DISCUSSION

To invert the data we used the code Res2D-Hu, developed by Prácser. 2D models for Dp and new configurations are shown in Figures 3 and 4. In most of the model independently from its dipping all data sets were able to detect the graphite rod which was embedded in sand and the dipping did not seem to influence the results significantly. In case of the largest dipping (30°) however the γ11n arrays showed a clearer image or only they could present the model body.

Anomalies associated with the boundaries of sand box are probably connected to its side and are real anomalies. The Dp array presented the interface between the sand box and the soil well, while the other arrays have no sufficient data points in that region. That's why at the side interfaces are not observed in their image. It is however not important in the present study, therefore we disregard these anomalies for further discussion.

There is a clear anomaly in each section at the horizontal position of the rod which is clearly separated both horizontally and vertically. Unexpected electrical model is obtained only from the γqnull array. All other array data produces correct position of the rod. The anomaly reaches the surface and thus top boundary of the conducting rod is not delineated by the Dp array data. In the image obtained from the γ11n arrays the top of the conducting body is moved upwards with only maximum 5 cm error.

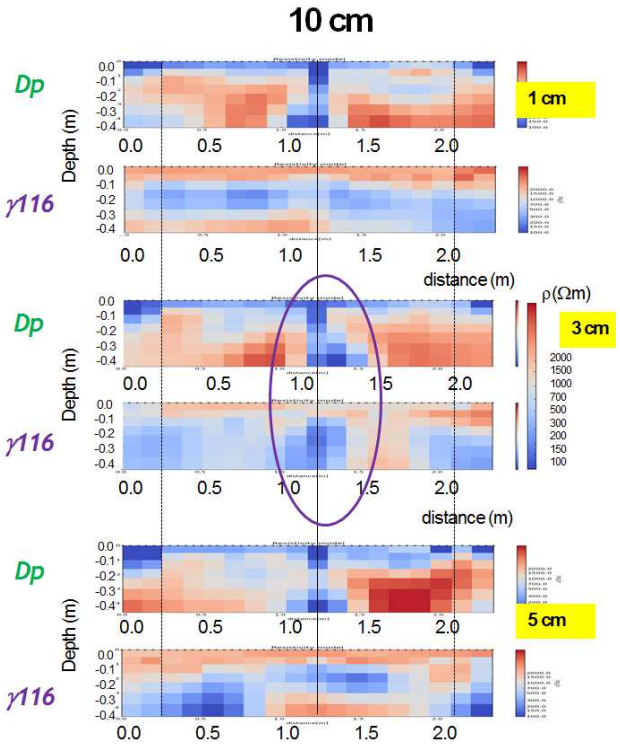

Figure 3: Geoelectrical model obtained from the 2D inversion of ERT profiles. The lower side of the dipping conducting rod is buried at 10 cm depth. Dp and γ 116 results are presented.

In the γ images there are other large size anomalies. The one at about 0.5-1 m appears on all γ images. These anomalies need to be interpreted using synthetic modelling experiments. The smaller size anomalies in the right side of the section may be 3D effects. By comparing the 2D electrical resistivity models obtained from the different array data, it can be said that the γ114 array provided the results closest to the true model in terms of the upper and lower boundary of the conducting rod with the greater resolution.

Figure 4 demonstrates that γ116 array could much better delineate the model vertically than the Dp one. In case of 20 cm depth even it is questionable that the Dp arrays are able to detect the anomaly, while it is clearly displayed by the γ116 array.

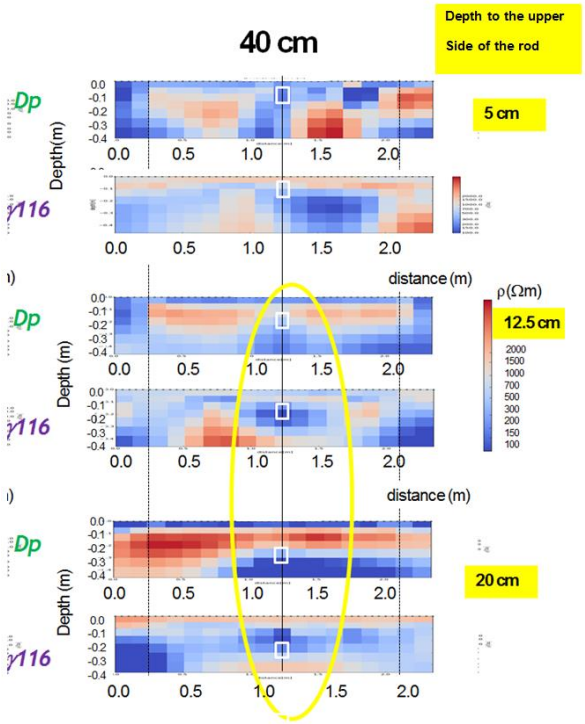

Figure 4: Geoelectrical model obtained from the 2D inversion of ERT profiles. The lower side of the dipping conducting rod is buried at 40 cm depth. Dp and γ116 results are presented.

CONCLUSIONS

There is a clear anomaly in each section at the horizontal position of the rod which is clearly separated both horizontally and vertically. Only the image of the γqnull array is somewhat strange in terms delineating geometry of the body. Vertically the Dp reaches the surface not giving an upper limit to its position. The γ11n arrays could delineate the model both horizontally and vertically with minimal shifts. Present study concludes that the combination of traditional and the γ arrays are the best to delineate the model geometry.

ACKNOWLEDGEMENTS

This work is carried out during Dr Sandor S., MTA CSFK Geod´eziai ´es Geofizikai Int´ezet, Hungary visit to IIT Roorkee, India; under Indian (INSA) and Hungarian Academies, in the frame of the Bilateral Agreement program. We are thankful to Dr Sandor for his support and guidance provided at various stages of data acquisition and interpretation.

REFERENCES

Falco P., Negro F., Szalai S., Milnes E. 2013. Fracture characterisation using geoelectric null-arrays. Journal of Applied Geophysics 93 (2013) 33–42.

Keller G V, Frischknecht F C. 1966. Electrical methods in geophysical prospecting. Oxford: Pergamon Press.

Szalai, S., Kis, A., Metwaly, M., Lemperger I, Szokoli K. 2014a. Increasing the effectiveness of electrical resistivity tomography using 11n configurations. Geophy. Prosp. 63/2. 508-424.

Szalai, S., Koppán, A., Szokoli K., Szarka, L. 2013. Geoelectric imaging properties of traditional arrays and of the optimized Stummer configuration. *Near Surface Geophysics, 2013,* **11**, 51-62.

Szalai, S., Lemperger I, Metwaly M, Kis Á, Wesztergom V, Szokoli K, Novák, A. 2014b. Multiplication of the depth of detectability using γ11n arrays. Journal of Applied Geophysics 107 (2014) 195–206.

Szalai, S., Szarka, L., Prácser, *E.*, Bosch, F.,Müller, I., Turberg, P. 2002. Geoelectric mapping of near-surface karstic fractures by using null arrays. Geophysics, Vol. 67/6,1769–1778.

Estimation of the anisotropy using CSRMT data in the transition zone of electric dipole

A. Shlykov[1], S. Agrahari[2], K. Antaschuk[3], A. Saraev[4], A. Simakov[5]
[1]St. Petersburg State University, Russia, shlykovarseny@gmail.com
[2]Indian Institute of Technology Kharagpur, India, sudha@gg.iitkgp.ernet.in
[3]St. Petersburg State University, Russia, antaschuk@gmail.com
[4]St. Petersburg State University, Russia, asaraev51@mail.ru
[5]St. Petersburg State University, Russia, sandhill@mail.ru

SUMMARY

The present work focuses on the estimation of anisotropy and its influence on the interpretation. Anisotropy of the subsurface is estimated using the transition zone measurements of Controlled-Source Radiomagnetotellurics (CSRMT) field measurements. In addition, the electrical resistivity measurements were also conducted The CSRMT results are compared with the electrical resistivity tomography data. The results of our anisotropic inversions are in good agreement with the existing theory. This has been verified by substituting the resistivity values, obtained from the electromagnetic and direct current inversion, in the theoretical equations. Results of anisotropic inversions are well correlated with the borehole data, well logging data and a priori information about the geology of the study area.

Keywords: Anisotropy, Controlled-source radiomagnetotellurics, Transition zone, Horizontal electric dipole.

Introduction

The “macro-anisotropy” phenomenon is known since the pioneer studies of Schlumberger brothers. The stack of thin layers, with contrast in resistivity values, is electrically equivalent to a single layer with the anisotropic resistivity and the thickness equal to the total thickness of the stack. Vertical and horizontal resistivities of equivalent layer have simple relation with the total horizontal conductance S and vertical resistance T of the stack (Maillet, 1947):

$$\rho_h = h_\Sigma / S \qquad \rho_v = T / h_\Sigma \tag{1}$$

Here ρ_h is horizontal resistivity, ρ_v is vertical resistivity, $S = \Sigma(h_i / \rho_i)$, $T = \Sigma(h_i \cdot \rho_i)$, $h_\Sigma = \Sigma(h_i)$, ρ_i is the resistivity of the i^{th} layer in the stack, h_i is the thickness of the i^{th} layer.

This anisotropy exists on the macroscale only because of the weak resolution of ground-based (surface) soundings. However, well logging measurements are able to resolve each thin layer independently. That is why this phenomenon is called “macro-anisotropy”.

Anisotropic layer has simple relations with isotropic equivalent. In the electrical resistivity measurements, conditions of equivalency are following:

$$\rho_{DC} = \sqrt{\rho_v \rho_h}, \qquad h_{DC} = \sqrt{\rho_v / \rho_h} \cdot h = \lambda \cdot h. \tag{2}$$

Here λ is coefficient of anisotropy. In the transverse flow of electrical current, such as plane wave magnetotellurics (MT) or loop-loop transient electromagnetics (TEM), conditions of equivalency are following:

$$\rho_{MT} = \rho_h, \qquad h_{MT} = h. \tag{3}$$

Therefore, two main conclusions can be derived: (i) in the anisotropic media we will obtain different resistivity for DC and EM methods and (ii) the thickness of anisotropic layer obtained by DC data will be λ times more than the actual thickness of the layer.

Horizontal electric dipole (HED) or grounded wire is a source of the EM field with complicated nature. In the near-field zone (Zonge, Hughes, 1991), the nature of the primary EM field is equivalent to DC case i.e. galvanic mode of the EM field. In the far-field zone, the primary EM field is the plane wave i.e. inductive mode. In the transition zone of the HED, EM field contains significant impact of both modes. Therefore, the measurements of the EM field in the transition zone of HED contain information about horizontal and vertical resistivities.

The controlled-source radiomagnetotelluric method (CSRMT) is a near surface electromagnetic frequency domain sounding, which measures the EM field of the vertical loop (Bastani, 2001) or the grounded wire (Saraev et al., 2017) in the frequency range 1-1000 kHz. In the urban regions, upper frequencies 10-1000 kHz can be covered by broadcast VLF-LF and AM radio transmitters

(McNeill, Labson, 1989; Tezkan, 2008). Usually, CSRMT surveys are conducted in the far-field zone of the controlled source for simplifying the inversion.

In this abstract, we are discussing the results of the field experiments of the CSRMT method (in the transition zone of the grounded wire) for the estimation of the macro-anisotropy. The resistivity values obtained from the CSRMT and ERT techniques are compared using equation (2).

Geology of the survey area

The survey area is located near St. Petersburg, Russia. The geology of the area is well studied during summer geological camps and it has horizontally layered structures with near to constant layer thicknesses. In the study area, the geological section contains following formations (from top to bottom):

1. Quaternary moraine loams (6-10 m);
2. Ordovician clayey limestones (11-13 m);
3. Ordovician shales (1 m).
4. Ordovician-Cambrian sandstones (10-15 m);
5. Cambrian blue clays (more than 150 m).

The most important characteristic of the geological section is alternation of thin more or less clayey sub-layers in the limestones. Between limestones and sandstones there is a thin layer of shales. It is illustrated by electrical well logging data obtained in the borehole drilled directly on the test area (Figure 1).This features will produce the macro-anisotropic response. The layer of clay was not reached by well but the top boundary of the clay is clearly observable on the nearby riverbed's slopes.

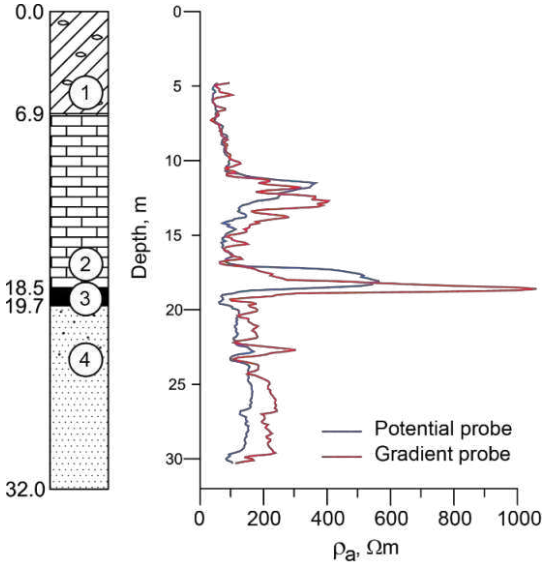

Figure 1. Geological column and electrical well logging data for the study area. 1 – moraine loams, 2 - clayey limestones, 3 - shales, 4 – sands.

Equipment

For CSRMT soundings, a digital EM receiver RMT-5 and portable AC transmitter GTS-1 was used (Saraev et al., 2017). The receiver was developed in St. Petersburg State University, and has five channels (two electric and three magnetic), total frequency band 1-1000 kHz and the 16 bit ADC. The RMT-5 receiver allows to use ungrounded (capacitive) electric antennas which significantly increase usability of the method. The GTS-1 transmitter has 1 kW output power, up to 300 V output voltage, 0.1-7.5 A output current and frequency band 0.1 Hz – 1 MHz. The transmitter is powered by portable gasoline generator. The squared wave output signal allows to use main harmonic of the signal and its higher odd subharmonics which increase the performance of the soundings.

For ERT measurements, the geophysical transmitter Astra-100 (Nord-West LLC, Moscow), receiver Medusa (SibGeophysPribor, Novosibirst) and digital commutator ComDD-2 (Geodevice LLC, St. Petersburg) were used.

Field experiment

The experimental survey layout is presented in Figure 2. For CSRMT measurements, two transmitters were placed orthogonal and independent to each other. The measurements were conducted along four lines of 200 m length each. The inter station spacing was selected 10 m and therefore 21 stations were measured along each profile line. The distance between the neighboring lines was about 50-70 m.

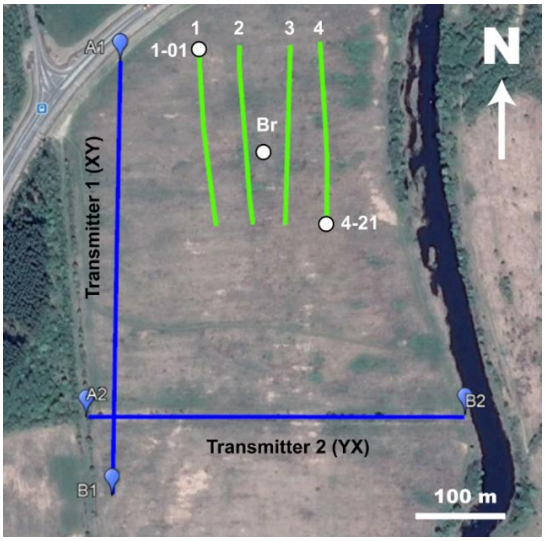

Figure 2. Survey layout. Green lines are the lines of measurements for CSRMT and ERT. Br – is borehole.

The receiver-transmitter distances were 80-220 m for Tx-1 orientated from South to North (XY direction) and 210-400 m for Tx-2 orientated from West to East (YX direction). Therefore, data from Tx-1 contains significant transition zone responses but the data from Tx-2 are mostly in the far-field zone (Figure 3). At each of the stations, we had three simultaneous measurements for frequencies 0.5, 5 and 50 kHz for Tx-1 and 0.45, 4.5 and 45 kHz for Tx-2. In the processing stage, we used up to 19th subharmonic for each main frequency. As a result, we have 27 points on the sounding curve from 1.5 to 950 kHz.

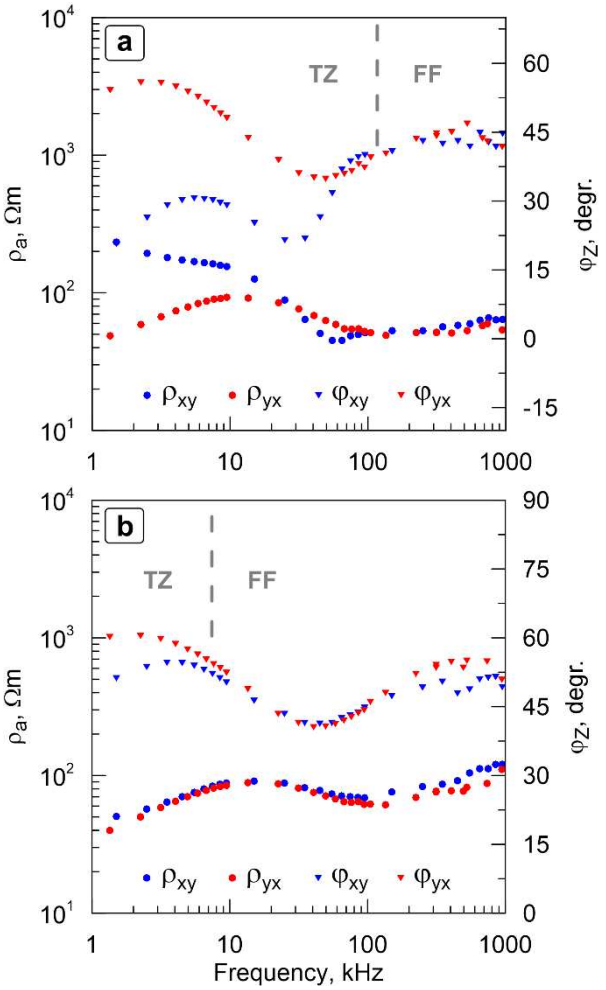

Figure 3. Example of the CSRMT data. **a** – line 1, station 5, **b** – line 4, station 5. TZ and FF stands for the transition zone and far-field zone of the source for φ_{XY} data, respectively.

Examples of the sounding curves for CSRMT stations 1-5 (line 1, station 5) and 4-5 (line 4, station 5) are presented in Figure 3. In both cases, the XY data contains transition zone response because of the closer distance to the source (80 and 220 m respectively). The YX data are totally in the far-field zone of the Tx-2 (distance 350 m). Very close data in the far-field for XY and YX direction prove the assumption of 1D geology. Certainly, the shallowest horizons are little bit more inhomogeneous and provide higher difference in XY and YX data at high frequencies. Small scattering of points along the sounding curve indicates high quality of measurements.

For electrical resistivity tomography, the pole-dipole array (forward and reverse) was applied. Distance between potential electrodes was equal to five meters. Maximum distance between current and potential electrodes was 120 m. This provides depth of investigation about 60 m.

Inversion and results

The 2D isotropic inversion of the ERT data is done by using the ZondRes2D software with smoothness-constrained stabilization functional by keeping uniform X-Z smoothing because of good density of data. The ERT inversion results are presented in Figure 4. Three-layer structure is clearly indicated: top layer with medium resistivity about 60 Ωm and thickness about 10 m (Quaternary loams), second layer with resistivity about 300-400 Ωm and thickness about 40 m (limestones and sands) and conductive basements (clay). Line 2 has interesting detail: the thickness of the resistive layer increases up to 50 m from South to North.

For anisotropic inversion of CSRMT data, we used the code described in Shlykov and Saraev, 2015. For this purpose, only XY impedance (ρ_{XY} and φ_{XY}) data along the Tx-1 is used because of strong transition zone response close to the source. We used 4-layer model based on the sounding curves. Results of the anisotropic 1D inversion are presented in Figure 5. We can see that only the third layer is anisotropic and this layer has thickness 22-27 m as expected by a priori geological information. Thickness of the anisotropic layer obtained from CSRMT data has little changes along the lines of measurement. The coefficient of anisotropy is λ = 1.3-1.7.

As we mentioned in the introduction, in the DC case the anisotropic layer has electrically equivalent and isotropic layer with thickness λ times bigger than thickness of the original anisotropic layer. In Figure 5, a comparison of the actual boundaries of the resistive layer obtained from the field ERT measurements (thick white dashed lines), the theoretical position of the bottom boundary of the resistive layer obtained from equation (2), and the anisotropic inversion results (thin pink lines) from the CSRMT method.

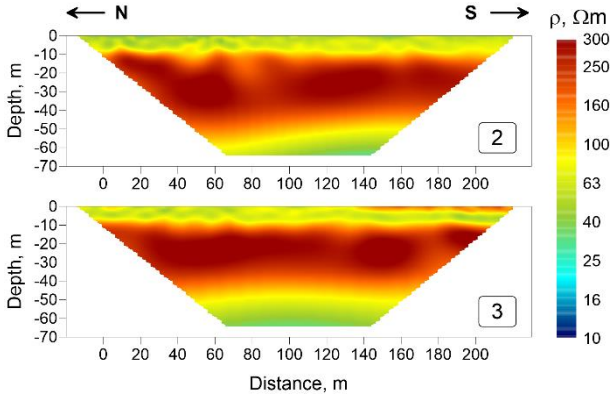

Figure 4. Results of the 2D inversion of ERT data for lines 2 and 3.

In general, the correlation between the thickness of the resistive layer obtained by ERT method and the theoretical thickness obtained by anisotropic inversion is very good. For line 2, the anisotropic layer has λ increase in thickness towards North. The same increment in the thickness is noticed in ERT results for the resistive layer. Here, we can conclude that the observed increase in the thickness in ERT result is an apparent increase. However, in reality only the vertical resistivity increases. This leads us to two possible geological interpretations. The increase in thickness might be attributed to either the lateral variation in the concentration of the clay particles in limestones or the lateral variation in the horizontal fracturing of the limestones.

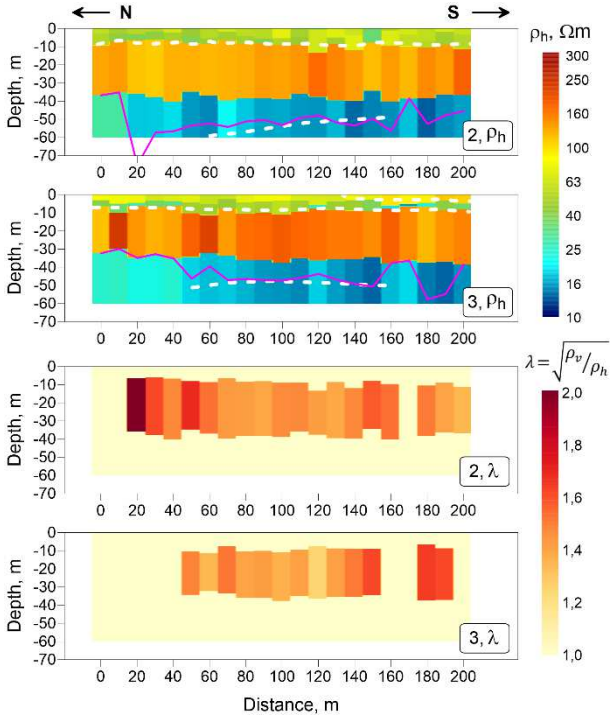

Figure 5. Results of the 1D anisotropic inversion of CSRMT XY data for lines 2 and 3. For details, refer to the text.

Conclusions

The results of the field experiment for estimation of the anisotropy of rocks using CSRMT method are presented and discussed. Anisotropic inversion algorithm is applied to the CSRMT data measured in the transition zone of the grounded wire. Inversion results for ERT and CSRMT data are significantly different in the thickness of the resistive macro anisotropic layer. The thickness obtained by ERT is 1.3-1.7 times larger than the CSRMT result. This mismatch has good agreement with the theoretical relations of the equivalent anisotropic and isotropic layers and partially proves the correctness of anisotropy obtained by CSRMT measurements.

Acknowledgements

This study was supported by the Russian Foundation for Fundamental Researches, project No 17-55-45042, and the Center GEOMODEL of St. Petersburg State University.

References

Bastani M. (2001) EnviroMT – a new Controlled Source/Radio Magnetotelluric System. PhD thesis, Uppsala University, 179 p.

Maillet R. (1947) The fundamental equations of electrical prospecting. Geophysics, 12, pp. 529–556.

McNeill, J.D., Labson V.F. (1989) Geological mapping using VLF radio fields, in Nabighian MN (ed) Electromagnetic methods in applied geophysics. Society of Exploration Geophysicists, Vol. 2, pp. 521–640.

Saraev A., Simakov A., Shlykov A., Tezkan B. (2017) Controlled-source radiomagnetotellurics: A tool for near surface investigations in remote regions. Journal of App Geophys, 146, pp. 228-237.

Shlykov A.A., Saraev A.K. (2015) Estimation the macroanisotropy of a horizontally layered section from controlled-source radiomagnetotelluric soundings. Izvestiya, Physics of Solid Earth, Vol. 51, No. 4, pp. 583-601.

Tezkan B. (2008) Radio magnetotellurics. Groundwater geophysics: a tool for hydrogeology. Reinhard Kirsch (ed.), Berlin; Heidelberg: Springer, pp. 295-318.

Zonge K.L., Hughes L.J. (1991) Controlled source audio-frequency magnetotellurics. Electromagnetic methods in applied geophysics. Vol.2 - App. Series: Investigations in geophysics, No 3, pp. 713-809.

Graphitic and Pyritic Black Schist and Black Shale
- Conduction Mechanisms in Highly Polarizable Rocks and Their Impact on EM Surveys

J.H. Börner[1], F. Girault[2], D. Kiyan[3], M. Bhattarai[4], L. B. Adhikari[4], V. Rath[3], F. Perrier[2] and K. Spitzer[1]
[1]Institute of Geophysics and Geoinformatics, Technical University Bergakademie Freiberg (Germany), jana.boerner@geophysik.tu-freiberg.de
[2]Institut de Physique du Globe de Paris, Sorbonne Paris Cité, Univ. Paris Diderot, CNRS, Paris (France)
[3]Dublin Institute for Advanced Studies, School of Cosmic Physics, Geophysics Section, Dublin (Ireland)
[4]National Seismological Centre, Department of Mines and Geology, Lainchaur, Kathmandu (Nepal)

SUMMARY

Electromagnetic measurement and data processing methods as well as numerical simulation and inversion techniques are getting more and more sophisticated. Thus, the requirements regarding spatial resolution, compositional classification and accuracy of interpretations increase. Consequently, there is room and necessity to investigate scenarios, where our classic understanding is insufficient and the mathematical treatment of electrical conductivity in terms of a scalar, real-valued quantity is inappropriate. This is the case, e.g., when electromagnetic field data become sensitive to highly polarizable rock formations, i.e. with a strongly frequency-dependent, complex conductivity. Besides ore mineralization zones, also black schist and black shale formations can bear such anomalous electrical properties, which can become relevant for large scale surveys even if they occur only in thin bands or layers.

Laboratory measurements of the frequency-dependent, complex-valued electrical conductivity of rock samples supported by accompanying tests such as, e.g., mineralogical analysis or scanning electron microscopy are able to fundamentally reveal the dominant conduction and polarization mechanisms. If strong polarization is present, its associated frequency range can be estimated and, thus, its relevance for a certain electromagnetic method can be assessed. The significance of laboratory results has been increased through recent developments in equipment, which now allow for measuring the complex conductivity over nine decades ranging between 10 000 s and 100 kHz. We present laboratory results from two areas, where electromagnetic field data are suspected to be affected by polarization phenomena in different frequency ranges.

The first area is the Main Central Thrust shear zone in the Himalayas of central Nepal, which was heavily affected by the deadly Mw7.8 Gorkha earthquake in 2015. Multiple magnetotelluric surveys have been conducted close to the shear zone, most of which indicate midcrustal conductive zones. We analyzed a graphitic and pyritic black schist outcropping in a CO_2-degassing area associated with the shear zone, thereby focusing on the nature of conduction and polarization as well as on anisotropy and salinity dependence of both plugs and crushed material. This black schist possesses an extraordinarily high polarizability and a highly frequency-dependent conductivity. The polarization is particularly pronounced at very low frequencies below 0.1 Hz. Moreover, the black schist is strongly anisotropic. Our investigations reveal that the main polarization feature is related to disseminated, aligned plates of graphite and suggest that magnetotelluric data recorded in the vicinity of the black schist could indeed be influenced by polarization phenomena.

The second investigated case is the anomalous appearance of the Moffat Shale Group in the Longford-Down area (Ireland) in airborne electromagnetic data (0.9 to 25 kHz). The Moffat Shale Group is a mudstone sequence of marine origin, which is rich in pyrite and partly also carbon. We have investigated the complex electrical characteristics of the shale with varying mineral composition and in dependence on the drilling direction to identify the substantial cause of the noticeably high apparent conductivity.

We further demonstrate by means of numerical modelling that neglecting the complex and frequency-dependent nature of conductivity can lead to serious artefacts in the inversion of electromagnetic field data if highly polarizable rocks are present. Ongoing investigations aim at the procedure of upscaling complex conductivity from laboratory to field scale.

Integrating resistivity into petroleum exploration on the Barents shelf: a geological perspective

Kim Senger[1]
[1]University Centre in Svalbard, kim.senger@unis.no

SUMMARY

The Norwegian part of the Barents shelf represents a frontier hydrocarbon province covering over 700 000 km^2 with 153 exploration wells drilled offshore to date. In addition, 17 exploration wells were drilled onshore Svalbard from 1963 to 1994. The Barents shelf has been severely uplifted during the Cenozoic, which led to significant impacts on the petroleum system; including source rock maturation, reservoir quality, trap and seal integrity and re-migration of hydrocarbons. Exploration well results nonetheless suggest a working petroleum system, with almost half of the exploration wells encountering hydrocarbons. Many of these, however, were technical discoveries in under-filled traps or with only residual gas remaining. One of the keys to exploration success on the Barents shelf is to make use of controlled source electromagnetic (CSEM) data to provide pre-drill estimates of pay zone resistivity and thus differentiate between low and high hydrocarbon saturation.

In this contribution, I first review the use of CSEM in exploration on the Barents shelf in the past decade focusing on case studies including the very shallow Wisting oil discovery, the sub-commercial Pingvin gas discovery and the recent CSEM-driven Kayak gas discovery. I subsequently present a comprehensive analysis of wireline data from offshore and onshore exploration wells, focusing on the geological controlling parameters on resistivity. Formation resistivity is primarily controlled by the presence and connectivity of electrically conductive fluids, i.e. brine. The matrix is usually insulating in sedimentary basins and resistivity is thus primarily controlled by: 1) porosity, 2) brine conductivity, 3) brine connectivity and 4) brine saturation. I illustrate how resistivity varies both vertically and laterally as a function of porosity reduction, and focus in particular on the resistivity contrast between hydrocarbon-bearing reservoir sandstones and the overlying source rock shales of varying quality and maturation levels.

Keywords: CSEM, MT, petroleum, Arctic, exploration

Synthesizing Seemingly Contradictory MT and Seismic Results to Image Thick Thermal Lithosphere beneath the Southeastern United States

Benjamin S. Murphy[1] and Gary D. Egbert
College of Earth, Ocean, and Atmospheric Sciences; Oregon State University; Corvallis, Oregon, USA
[1]murphybe@oregonstate.edu

SUMMARY

Although both seismic velocities and electrical conductivity are sensitive to temperature, thermal lithosphere thickness has been derived almost exclusively from seismic data; conductivity is often too strongly affected by small amounts of water (or some very conductive minor phase) to be a reliable indicator of temperature. However, elastic parameters are also influenced by factors beyond temperature, and sometimes MT provides the strongest constraint on mantle temperatures. An excellent example of this situation is found in the southeastern United States (SEUS), where EarthScope long-period MT data require high resistivities (>300 Ωm) to at least 200 km depth. As dry mantle mineral conduction laws provide an upper bound on temperature for an observed resistivity value, the only interpretation is that lithospheric (<1330°C) temperatures persist to 200 km. However, both surface wave and body wave tomography imply that seismic velocities in this region are not particularly fast, which has led to the widespread view of a relatively thin (<150 km) thermal lithosphere beneath the SEUS. We show that both MT and seismic results are consistent with a thick (180-200 km) thermal lithosphere. Reduced seismic velocities (relative to cratonic regions) can be explained by taking into account the effect of finite grain size (anelasticity). Predicted seismic velocity as a function of temperature is slower when including anelastic effects, even at reasonable grain sizes of 1-10 mm; this permits mantle temperatures that are colder than would typically be inferred. Agreement between MT and seismic results is further improved by considering variations in oxygen fugacity, which generally decreases with increasing pressure. This translates to a decrease in the number of charge carriers with increasing depth and allows warmer temperatures than would otherwise be inferred from the observed resistivity. Clearly the interpretation based on seismic data alone is not consistent with all available data, but by taking into account these intrinsic controls on the complementary geophysical observables we can arrive at a meaningful and coherent picture of lithospheric properties.

Keywords: Joint interpretation, mantle temperature, lithosphere

An upper bound on the electrical conductivity of oceanic mantle at the limit of hydration: the role of pyroxenes

S. Naif
Lamont-Doherty Earth Observatory, Columbia University, snaif@ldeo.columbia.edu

SUMMARY

Marine magnetotelluric studies often detect elevated electrical conductivity in the asthenosphere. Such observations require invoking either a small fraction of water stored in nominally anhydrous minerals or low degrees of interconnected partial melt. This non-uniqueness is complicated by significant disagreements between independent laboratory measurements on the conductivity of hydrous olivine. Existing MT studies often utilize only one of the competing empirical conductivity models of hydrous olivine for interpretation purposes, which can be problematic since in many cases the interpretation depends on the choice of which model to apply. Furthermore, this approach inherently assumes an olivine-only mantle composition and ignores the role of pyroxenes as well as thermodynamic stability. In an effort to better distinguish between hydration and partial melt, this study combines plate cooling models with the solidus of hydrous peridotite to estimate an upper bound mantle conductivity at the limit of hydration, taking into account the contribution of pyroxenes. Conductive and resistive end-member empirical conductivity models are applied. The results show partial melt is the only viable interpretation to explain mantle conductivity beneath young plates regardless of model choice. For observations beneath older plates, the resistive end-member model requires hydration levels consistent with MORB values (<200 ppm) while the conductive end-member predicts nearly dry mantle (<20 ppm). In scenarios where the hydration estimates are geologically plausible, as is the case for mantle conductivity beneath older plates, partial melt remains a viable alternative interpretation. The hydration estimates diverge dramatically and become unrealistic when pyroxene is ignored, increasing by a factor of five for the resistive end-member and decreasing by a factor of two for the conductive end-member model.

Keywords: Oceanic mantle conductivity, hydration, role of pyroxenes, origin of asthenosphere

Azimuthal anisotropy in 33 Ma Pacific lithosphere

C. Chesley[1], K. Key[2], S. Constable[3], J. Behrens[4] and L. MacGregor[5]
[1,2]Lamont-Doherty Earth Observatory, [1]chesley@ldeo.columbia.edu, [2]kkey@ldeo.columbia.edu
[3,4]Scripps Institution of Oceanography, [3]sconstable@ucsd.edu, [4]jb@cdip.ucsd.edu
[5]Rock Solid Images, lucy.macgregor@rocksolidimages.com

SUMMARY

The anisotropic fabric of the oceanic lithosphere yields insights into the processes involved in plate formation and evolution. Here we examine the electrical anisotropy of 33 Ma Pacific lithosphere using controlled-source electromagnetic data collected during the Anisotropy and Physics of the Pacific Lithosphere Experiment (APPLE). The APPLE cruise included a 30 km radius circular deep-tow of a horizontal electric dipole (HED) transmitter around orthogonal pairs of HED receivers to measure azimuthal anisotropy and a radial tow to 70 km range to measure the resistivity structure as a function of depth. Major and minor axes of polarization ellipses computed from the circular tow data show strong 2θ and 4θ azimuthal dependence, which indicates a robust azimuthal anisotropy in the oceanic lithosphere. We performed a nonlinear anisotropic inversion of these data for horizontal transverse isotropy, with the vertical plane of isotropy aligned orthogonal to the paleo-spreading direction. Our best model constrains conductivity to about 20 km depth and shows at least an order of magnitude of anisotropy between the paleo-spreading and paleo-ridge directions in both the crust and uppermost mantle. In the crust, conductivity is higher in the paleo-ridge striking vertical plane; the opposite is true in the uppermost mantle, where conductivity is higher in the paleo-spreading direction. We propose that the crustal anisotropy results from seawater infiltration or conductive alteration minerals in deep cutting normal faults that formed during paleo-extension of the young crust. The uppermost mantle anisotropy is consistent with a shear-aligned fabric frozen in as the plate cooled. This may have resulted from crystal preferred orientation of olivine or alignment of a conductive mineral phase along grain boundaries.

Keywords: azimuthal anisotropy, oceanic lithosphere, shear-aligned fabric

INTRODUCTION

Electrical conductivity anisotropy denotes a variation in the conductivity of a material with direction. In geophysical studies, anisotropy may result from microscopic properties inherent to a mineral or mineral-scale fabrics that induce a lattice or crystal preferred orientation (Karato et al, 2008); it may also arise from macroscopic scale features such as fault-enhanced hydration pathways (Key et al, 2012) that promote alteration. Observations of the direction, magnitude and depth dependence of anisotropy can be used to infer the mechanisms at work during lithospheric formation and aging. For instance, anisotropy aligned with ridge normal faults can inform us of the extent to which hydration permeates the lithosphere whereas anisotropy aligned with the paleo-spreading direction may suggest the importance of shear in early plate formation. The nature and sense of lithospheric anisotropy is paramount to understanding dynamic processes associated with plate formation and evolution.

Little is known about the electrical anisotropy of oceanic lithosphere due to a paucity of field research. Magnetotelluric (MT) studies have shed light on electrical anisotropy in the asthenosphere (Naif et al, 2013), yet deep-ocean MT data are typically insensitive to the shallower depths of the resistive crust and uppermost mantle. Here we report inversion results of controlled-source electromagnetic (CSEM) data, which are highly sensitive to the electrical structure in the crust and upper 20 km of the mantle, collected over 33 Ma Pacific lithosphere. We show that, to fit the observed data, both the crust and uppermost mantle require azimuthal anisotropy.

A reversal in the direction of maximum conductivity offers insights into the nature of the oceanic lithosphere.

METHODS & RESULTS

The data for this study were collected during the Anisotropy and Physics of the Pacific Lithosphere Experiment (APPLE). The survey location is ∼1000 km west of San Diego, CA in a region where the fossil spreading direction is approximately east-west (Figure 1). North-south trending escarpments in the area indicate high-angle normal faulting.

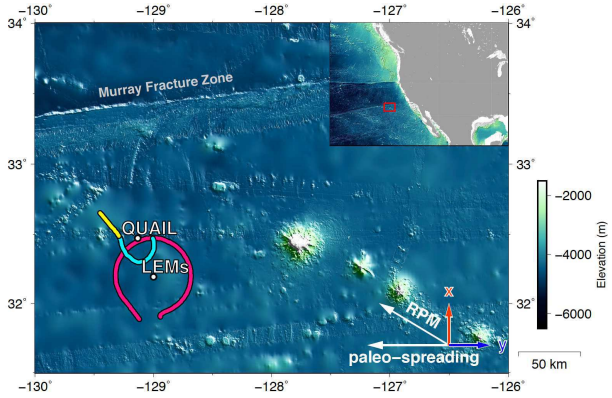

Figure 1: Map of APPLE survey area. White circles denote locations of the EM receivers, Quail and the LEMs, whose data were used for inversion. The transmitter tow path is colored by the azimuthal (pink), radial (yellow), and semi-circular (blue) tow. RPM = relative plate motion direction.

We collected CSEM data by deep-towing a horizontal electric dipole (HED) while transmitting an EM wave with a fundamental frequency of 3.9889 Hz. To measure azimuthal anisotropy, the APPLE survey included a 30 km radius circular and 15 km radius semi-circular deep tow around orthogonal pairs of HED receivers, with electric field sensors on the perimeter and long-wire electric field receivers (LEMs) in the center of the large circular tow (Figure 1). Data collected during a radial tow ranging from 14 to 70 km provides constraints on the depth dependence of conductivity (Figure 1).

The raw time series data were Fourier transformed and stacked to yield amplitudes and phases at the 3.9889 Hz fundamental harmonic (Behrens, thesis).

The vector electric field recorded at each receiver has an associated polarization ellipse that can be decomposed into its maximum and minimum amplitudes, P_{max} and P_{min}, respectively. When the transmitter is towed azimuthally around a centrally located receiver and the conductivity is isotropic and laterally uniform, P_{min} = 0 for all transmitter-receiver azimuths. Conversely, azimuthally anisotropic or laterally varying conductivity can produce non-zero P_{min} data. Plotting P_{max} and P_{min} as a function of azimuth with respect to the LEM receivers from our APPLE data elucidate that the underlying lithosphere is anisotropic (Figure 2). In particular, our data show a strong 2θ symmetry in P_{max} and 4θ symmetry in P_{min}, suggesting azimuthal anisotropy is significant. Further, the symmetry in the observed data suggests that significant lateral variations in conductivity can be ruled out.

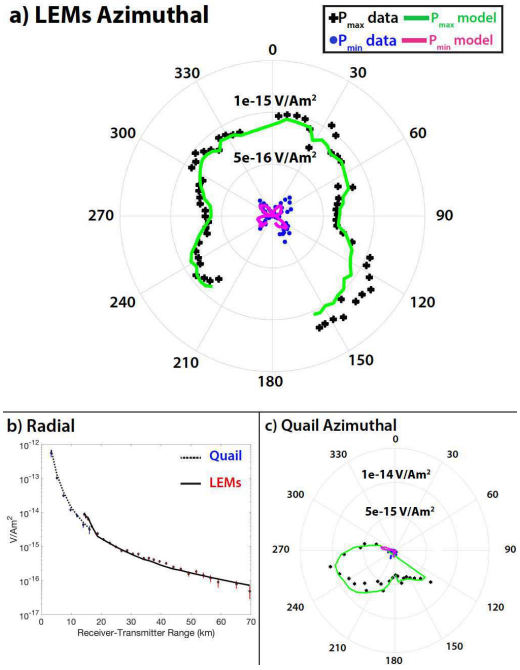

Figure 2: Fit of preferred resistivity model to data. a) Azimuthal dependence of P_{max} and P_{min} for the azimuthal tow data recorded by the LEM receivers. b) Radial data recorded by the LEM and Quail receivers. c) Quail data from the semi-circular tow.

We constructed a layered resistivity model and carried out a nonlinear anisotropic inversion of the azimuthal and radial mode data assuming transverse isotropy with the vertical (xz) plane of isotropy aligned orthogonal to the paleo-spreading

(y) direction. Our inversion penalized sharp resistivity jumps across boundaries and anisotropy within layers (Key, 2016). Our preferred model (RMS misfit≈1.36) shows a highly anisotropic crust ($\rho_y/\rho_{x\ upper}$ ∼18; $\rho_y/\rho_{x\ lower}$ ∼36) and uppermost upper mantle (ρ_x/ρ_y ∼29) with the opposite senses of anisotropy (Figure 3). Fits of this model to the data are provided in Figure 2.

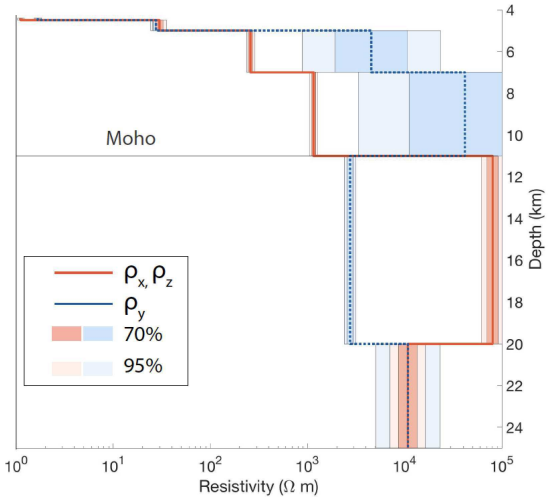

Figure 3: Preferred resistivity model with 70% and 95% confidence intervals from a linearized uncertainty analysis.

DISCUSSION

We interpret our results in the framework of relevant geophysical and geological studies on oceanic lithosphere (Figure 4).

Crustal Anisotropy The crustal anisotropy of our preferred model ranges from 18x (lower crust) to 36x (upper crust) with conductivity highest in the ridge-parallel direction. Everett and Constable (1999) show this pattern to be consistent with conductive, vertical sheets. As north-south trending escarpments in the seafloor bathymetry present evidence for normal faulting in the area, we propose the anisotropy may indicate that such faults acted as fluid pathways that permitted hydration into the upper and lower crust, either in the form of free-water in pore-spaces created by faulting or through the formation of conductive alteration minerals.

The models of Korenaga (2007) show that ridge-parallel vertical cracks extending to depths of 10-30 km in 10-100 Ma lithosphere can open due to thermal stress accumulation in cooling lithosphere. Were these cracks to form they would permit seawater and sediments to infill vertical planes, leading to an increased conductivity in the paleo-ridge parallel direction, which is compatible with our preferred model. Analysis of crustal sections collected at the Hess Deep Rift show evidence of dike-parallel fault widening with time (Varga et al, 2004). Such widening should increase porosity of the sheeted dike section and lead to an increase in conductivity of the upper crust in planes parallel to dikes. Additional evidence for such faulting is seen in the Troodos ophiolite where extensional fractures penetrated the sheeted dike region (Varga et al, 2004). These vertical faults appear to have permitted hydrothermal fluid focusing, which resulted in epidotization parallel to the faults. We suspect hydrothermal alteration to have affected the APPLE crust. Thus conductive alteration minerals like epidote that formed along dike parallel fractures may help account for the crustal anisotropy we have modeled.

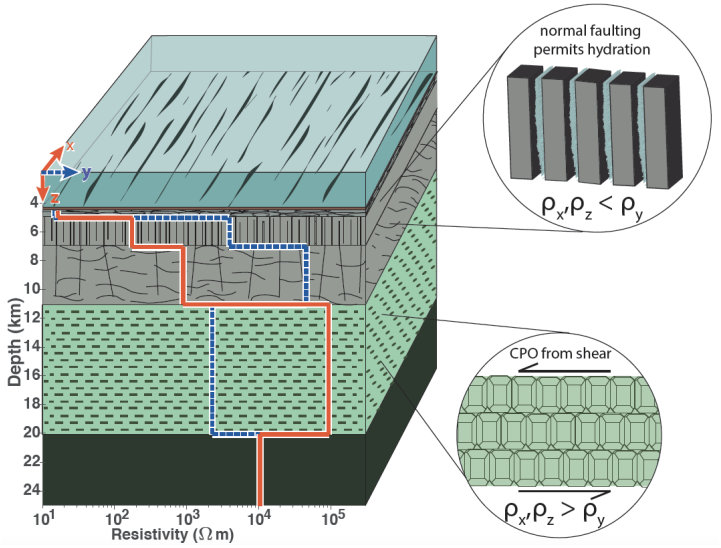

Figure 4: Geological interpretation of preferred resistivity model.

*Uppermost Mantle Anisotropy*å In the uppermost mantle, the paleospreading direction is ∼29x more conductive than the paleo-ridge parallel vertical plane. Everett and Constable (1999) show that this pattern can be generated by horizontally aligned conductive rods. We propose that this higher conductivity is related to the deformation history of the uppermost mantle, specifically as it underwent shear strain early in its lithospheric formation.

Measurements on olivine, reveal significant anisotropy in the presence of water (Dai and Karato, 2014; Yoshino et al, 2006) and upon shearing (Pommier et al, 2015). Seismic anisotropy shows that the [100] axes of olivine align subparallel to the shear direction under shallow lithospheric conditions (Karato et al, 2008), and conductivity studies reveal that water will cause the [100] axis to become the most conductive direction in olivine (Dai and Karato, 2014; Yoshino et al, 2006). However an intrinsic anisotropy of only $\sim$2.7x is found in lab studies (Dai and Karato, 2014) and thus our data require additional mechanisms to explain the observed anisotropy.

Pommier et al (2015) found that a shear strain of $\gamma \sim 3.5$ on olivine aggregates resulted in a factor of 10 increase in conductivity parallel to the shear direction. Though this is not as large as the anisotropy observed in our model, it is significantly larger than lab studies on undeformed olivine, which suggests shear must be important in the formation of the uppermost mantle. Another possible contributor to uppermost mantle anisotropy is the interconnection of a conductive mineral phase along grain boundaries (Everett and Constable, 1999). Duba and Shankland (1982) suggest that, so long as graphite ($\sim 10^5$ S/m at lithospheric temperatures) or solid carbon is abundant ($>$100 ppm), stable, and interconnected, it could explain high conductivities in the mantle. Sulfide minerals, which also have a higher conductivity than peridotites, have already been found along grain boundaries and fractures in peridotitic xenoliths (Ducea and Park, 2000). Either or both of these phases may play a role in mantle anisotropy.

CONCLUSIONS

Our preferred model from anisotropic inversions of CSEM data collected on 33 Ma Pacific lithosphere shows electrical anisotropy in the oceanic crust and uppermost mantle. The crustal anisotropy (18x-36x) consists of a more conductive vertical plane striking in the paleo-ridge direction. This is consistent with vertical, paleo-ridge parallel, conductive sheets and may indicate seawater infiltration or mineral alteration. The uppermost mantle anisotropy (29x) has a more conductive paleo-spreading direction, which likely represents the preservation of shear strain on olivine caused by paleo-flow in the uppermost mantle and/or the strong alignment of a conductive mineral phase, potentially due to shear strain as well.

REFERENCES

Dai L, Karato S (2014) High and highly anisotropic electrical conductivity of the asthenosphere due to hydrogen diffusion in olivine. Earth Planet Sci Lett 408:79–86

Duba AG, Shankland TJ (1982) Free carbon and electrical conductivity in the earth's mantle. Geophys Res Lett 9:1271–1274

Everett ME, Constable S (1999) Electric dipole fields over an anisotropic seafloor: Theory and application to the structure of 40 Ma Pacific Ocean lithosphere. Geophys J Int 136:41–56

Karato S, Jung H, Katayama I, Skemer P (2008) Geodynamic significance of seismic anisotropy of the upper mantle: New insights from laboratory studies. Ann Rev Earth Planet Sci 36:59–95

Key K (2016) MARE2DEM: A 2-D inversion code for controlled-source electromagnetic and magnetotelluric data. Geophys J Int 207:571–588

Key K, Constable S, Matsuno T (2012) Electromagnetic detection of plate hydration due to bending faults at the middle america trench. Earth Planet Sci Lett 351–352:45–53

Korenaga J (2007) Thermal cracking and the deep hydration of oceanic lithosphere: A key to the generation of plate tectonics? J Geophys Res 112:1–20

Naif S, Key K, Constable S, Evans R (2013) Melt-rich channel observed at the lithosphereâĂŞasthenosphere boundary. Nature 495:356–359

Pommier A, Leinenweber K, Kohlstedt DL, Qi C, Garnero EJ, Mackwell SJ, Tyburczy JA (2015) Experimental constraints on the electrical anisotropy of the lithosphere-asthenosphere system. Nature 522:202–206

Varga RJ, Karson JA, Gee JS (2004) Paleomagnetic constraints on deformation models for uppermost oceanic crust exposed at the Hess Deep Rift: Implications for axial processes at the East Pacific Rise. J Geophys Res 109:1–22

Yoshino T, Matsuzaki T, Yamashita S, Katsura T (2006) Hydrous olivine unable to account for conductivity anomaly at the top of the asthenosphere. Nature 443:973–976

Study on complex resistivity of artificial sandstone containing conductive mineral under high pressure

Gang Tian[1], XingongTang[2*], Kui Xiang[3] and Meiyao Chi[4]
[1]Yangtze University, Wuhan , China, 1053390444@qq.com
[2]Yangtze University, Wuhan , China, Corresponding author：tangxg@yangtzeu.edu.cn
[3]Yangtze University, Wuhan , China, cjdxxk@163.com
[4]Yangtze University, Wuhan , China, 411476077@qq.com

SUMMARY

The sandstone samples with different mineral content and volume content were artificially synthesized by using brass powder, pyrite sand, graphite powder, epoxy resin, etc. Complex resistivity measurements were taken to the samples by using AutoLab-1000 equipment under different formation pressure conditions. The complex resistivity and the parameters of zero frequency resistivity, polarizability, and constant time of the artificial sandstone standard were derived based on the Debye decomposition model. Made a discussion of the relationship between the parameters of the model, the volume content of conductive minerals, connectivity, formation pressure and other factors. The research results are of great significance for understanding the electrical characteristics of artificial sandstone samples under high pressure.

Keywords: Artificial sandstone Polarizability Complex resistivity Formation pressure Debye model

INTRODUCTION

The induced polarization effect refers to the phenomenon of secondary electric field that slowly changes with time which due to the electrochemical action of underground rock under the action of an external electric field. After the 1960s, the induced polarization method has gradually become the main exploration method for finding various metal deposits.Some scholars have simulated the frequency dispersion of rocks through equivalent circuits and proposed different models (Pelton 1978;Nordsiek, 2008;). Based on different models, inversion complex resistivity can extract the spectrum parameters of the rock. A large number of scholars have studied spectral parameters such as polarizability, resistivity, and constant time (Zhang Saizhen et al.1984; Xiao Zhanshan et al.2009;). But these research mainly focus on the natural rock samples. Due to the complex inside pore structure of the natural samples, the non-uniformity of the skeleton composition, and the phase state difference of the multi-fluid, the results of the theoretical model and the actual measurement may be quite different. A few scholars have conducted research on artificial rock samples(Liu, Zhuping et al.1994; Huang, Lianshan et al.2014). However, there are few reports on the analysis results of artificial sandstone samples and the experiments on artificial rock samples which under high pressure have hardly been done.In this paper,conducted complex resistivity measurements on artificial sandstone samples under different formation pressure conditions. Using Debye decomposition model, the complex resistivity parameters of rock samples are obtained.The spectrum parameters and their influencing factors under different pressure conditions were analyzed and discussed.

METHODS

The artificial samples of this experiment were mainly made by conductive minerals such as brass powder, pyrite sand, etc.The experimental system is AutoLab-1000 equipment and SI-1260 impedance analyzer. The test confining pressure -hole pressure are total of seven groups(5-2Mpa, 10-5Mpa, 15-5Mpa, 20-5Mpa, 30-5Mpa, 40-5Mpa, 50-5Mpa). The measurement frequency is in the range of 0.01Hz to 10000Hz, and the test temperature is room temperature. The polarization above 100 Hz is dominated by the Maxwell-Wagner polarization which is generated in the multiphase interface within the rock, But the polarization below 100 Hz is mainly the electric double layer effect which is generated by the Interaction of rocks and electrodes and pore fluids. The electric double layer effect is the primary concern of the experiment.In this paper,the parameters of complex resistivity were derived based on the Debye decomposition model.

EXAMPLES

In this paper,nine artificial sandstone samples were tested in the experiment. Table 1 shows the basic physical properties of the rock samples.

Pure sandstone sample

Figure 1 shows the measurement results of pure sandstone artificial sample(Yn-0) under different pressure. It can be seen from Figure 1 that the pure sandstone standard sample has a higher resistivity value,the resistivity and polarizability are increased with the increase of pressure difference.The constant time is small, and the peak value appears first and then decreases gradually with the increase of the pressure difference.The reason is that as the confining pressure continues to increase, the fluid in the pores is gradually exhausted, resulting in an increase in the resistivity value. At the same time, the induced polarization effect of pure sandstone is dominated by ionic conductor. As the confining pressure increases, the pores are continuously compressed, resulting in an increase of the specific surface area of the liquid, which finally results in an increase of the polarization effect.

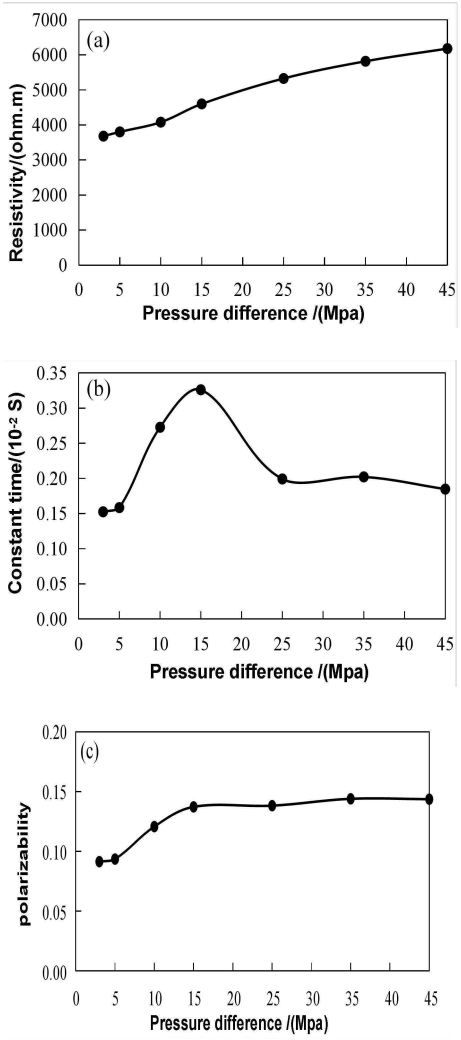

Figure 1. Measurement results of pure sandstone sample(Yn-0) under different pressure

Brass powder samples

Figure 2 shows the results of three brass powder samples with different mineral volume contents (see Table 1). It can be seen from Figure 2a, the lower the brass powder volume content, the greater the differential pressure and the higher the resistivity. The constant time also has a positive correlation with the pressure difference as a whole (Figure 2b). The polarizability increases with the volume content of the mineral and the pressure difference (Figure2c).Metal minerals brass powder samples have poor connectivity, large porosity, and the induced polarization effect is dominated by ionic conductors. Therefore, as the confining pressure increases, the pores are compressed and the pore fluid is discharged, resulting in an increase of the resistivity and the specific surface area of the liquid,which finally results in an increase of the polarizability.

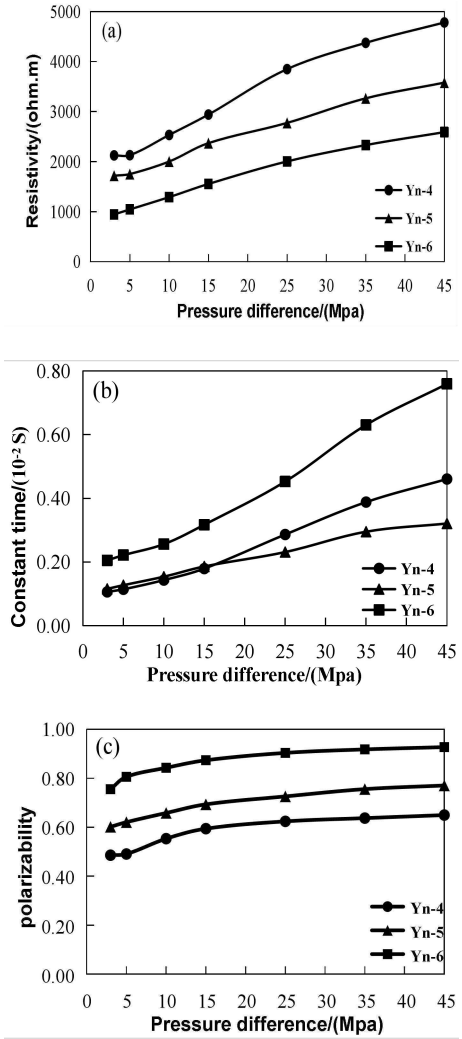

Figure 2. Measurement results of brass powder samples under different pressure

Pyrite samples

The spectral characteristics of pyrite specimens are relatively complex.From Figure 3, it can be seen

that when the pyrite content is low (<15%), the resistivity increases with the increase of pressure difference; On the contrary,when the pyrite content is high, the bigger the pressure difference ,the lower the resistivity. This is due to the fact that when the pyrite content is low, the conductivity is dominated by pore fluids (ionic conductors). However when the pyrite content is high, the conductivity is dominated by metal particles. For ion conductors, as the confining pressure increases, the pores are compressed and the pore fluid is expelled, resulting in an increase in resistivity. At the same time, the pressure increases the liquid specific surface, so the polarizability increases. But for metal conductors, pressure makes the metal particles more connected, resulting in a decrease of resistivity and polarizability. The constant time is related to the pressure difference and the content of conductive minerals. When the pyrite content is low (<15%), the constant time decreases with the increase of the volume content of the mineral and increases with the pressure difference; On the contrary,when the pyrite content and the confining pressure is high, the constant time increases first and then decreases. The larger the pressure difference, the smaller the τ value.

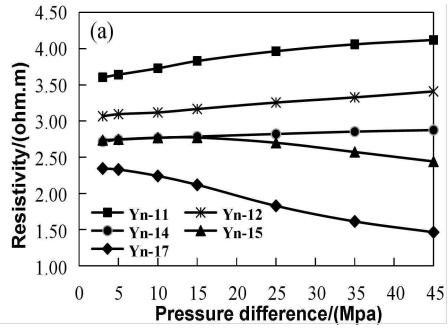

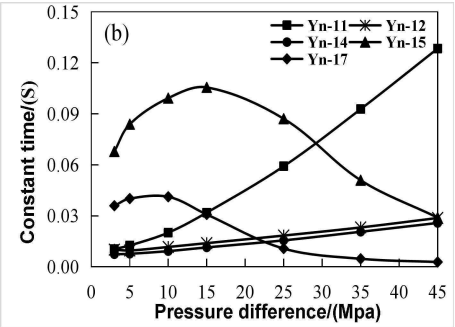

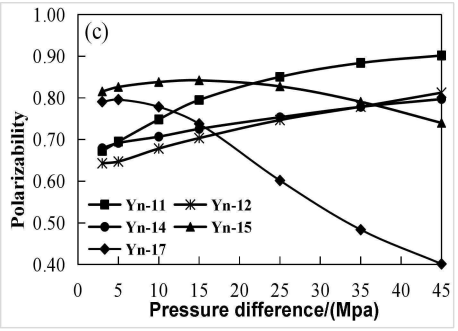

Figure 3. Measurement results of pyrite samples under different pressure

Some scholars have done research on the influencing factors of constant time.Pelton (1978) found that mineral composition has no fundamental effect on the value of τ . Zhang Saizhen (1984) believes that only when the conductive minerals volume is high enough, the mineral composition will show its influence on the τ .We analyzed the experimental results of artificial samples for different mineral compositions. Figure 4 shows the comparison of the constant time with the size of the mineral particles.

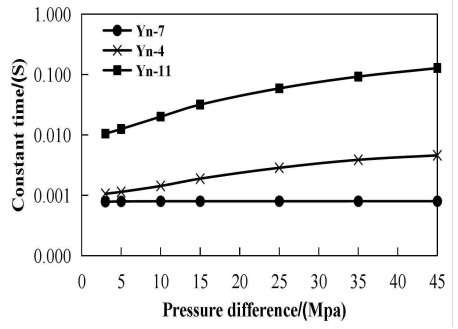

Figure 4. Comparison of constant time and mineral particle size

It can be seen from Fig. 4 that when the conductive minerals have the same volume content and formation pressure, while the content is not high and the rock sample structure is similar, the larger the mineral particles, the greater the value of τ .It shows that the size of mineral particles has a certain influence on the constant time.

CONCLUSIONS

Through experiments and analysis, the following conclusions were obtained:

(1) The rock resistivity is related to the volume content of metal minerals and connectivity of metal particles and formation pressure. In the case of rock samples that do not contain metal minerals or the metal minerals have poor connectivity, the resistivity increases as the formation pressure increases. On the contrary, while rock samples with better connectivity, the higher the formation

pressure, the lower the resistivity.

(2) The time constant is related to formation pressure and conductive mineral particle size and connectivity. The larger the mineral particles, the greater the value of τ .For sandstone samples with less conductive mineral content and poor connectivity, the greater the formation pressure, the greater the value of τ .

(3) When the metal particle connectivity is good, the higher the volume content of the conductive mineral and the higher the formation pressure, the lower the polarizability. On the contrary, for rock samples with poor connectivity, the greater the formation pressure, the greater the polarizability.

Acknowledgement

This work is supported by Chinese National Natural Science Fund (41674107, 41574064, 41404087) and Chinese National Program for key Research and Development(2017YFB0202904) .

REFERENCES

Huang Lishan,Jing Rongzhong,Zhang Shengye et al.Research on complex resistivity of rock model[J].Progress in Geophysics,2014,29(06): 2657-2664.

Liu Zhuping,Wu Xiaowei, Chu Zehan, Experimental Measurement and Research of Rock Acoustic Parameters[J],Chinese Journal of Geophysics, 1994,37(5):659-666.

Sven Nordsiek,Andreas Waller. A new approach to fitting induced-polarization spectra[J]. Geophysics2008,73(6):235-245.

W. H. Pelton, S. H. Ward, P. G. Hallof, Mineral discrimination and removal of inductive Coupling with multifrequency IP,Geophysics,1978,43(3) :588-609.

Xiao Zhanshan,Zeng Zhiguo,Zhu Shihe et al.Experimental study on the evaluation of wettability based on the dispersion properties of rock electrical parameters[J].Chinese Journal of Geophysics,2009,52(05):1326-1332.

Zhang Saizhen,Li Yingxian,Zhang Shuzheng et al.Frequency characteristics and influencing factors of low-frequency electrical phase of rock several metal ore fields in China[J].Chinese Journal of Geophysics,1984(02):176-189.

Rock sample number	Conductive mineral composition	Particle diameter /mm	Volume content /mm	height/ cm	Diameter /cm	Dry density /g/cm^3	Porosity/%
Yn-0	River sand: Epoxy resin =5:1			4.05	2.57	2.26	10.0
Yn-4	Brass powder	<0.2	5	3.99	2.57	2.74	13.0
Yn-5	Brass powder	<0.2	10	4.02	2.57	3.03	15.1
Yn-6	Brass powder	<0.2	20	3.45	2.57	3.63	13.8
Yn-11	Pyrite sand	<0.27	5	3.85	2.57	2.42	9.8
Yn-12	Pyrite sand	<0.27	7	3.80	2.57	2.57	10.0
Yn-14	Pyrite sand	<0.27	12	4.19	2.57	2.71	12.7
Yn-15	Pyrite sand	<0.27	15	3.89	2.57	2.85	9.8
Yn-17	Pyrite sand	<0.27	20	4.09	2.57	2.96	9.5

Table 1. Basic physical properties of the samples

The electrical structure beneath Harrat Rahat – crustal anisotropy in response to asthenospheric flow

P. A. Bedrosian[1], J. Peacock[1], M. Dhary[2], A. Sharif[2] and H. Zahran[2]
[1]U.S. Geological Survey, pbedrosian@usgs.gov, jpeacock@usgs.gov
[2]Saudi Geological Survey, dhahry.mk@sgs.org.sa, zahran.hm@sgs.org.sa

SUMMARY

The Kingdom of Saudi Arabia is transected by a series of Miocene and younger lava fields, termed 'harrats,' that cross the Neoproterozoic Arabian Shield and trend sub-parallel to the Red Sea spreading center. One of the largest of these fields, Harrat Rahat, extends for nearly 300 km. Its northern extent lies close to the city of Al Madinah, with historic flows (1256 AD) that reached within 20 km of the city. The Saudi Geological Survey has partnered with the United States Geological Survey to carry out a volcanic hazard assessment of the northern part of Harrat Rahat. This multi-disciplinary effort includes geological, geochemical, and geophysical investigations at a range of spatial scales. Geophysical investigations include a magnetotelluric survey designed to study the regional tectonic setting of Harrat Rahat, identify potential zones of partial melt within the crustal column, and delineate structures that may control the transport and emplacement of melt. Nearly 120 MT stations were collected over a 12,000 km^2 area covering the region of historic volcanism as well as the nearby city of Al Madinah.

Isotropic 3D inverse models image a thin volcanic section atop a shallow (< 1 km thick) conductor that partially overlaps a gravity low. This conductor may represent sediments below the volcanic rocks or alteration near the base of the volcanic section. Additional shallow conductors northeast of the Harrat correlate with sabkha (arid salt flat) deposits. The upper crust beneath the Harrat is generally resistive with no indication of melt storage.

In the lower crust, isotropic resistivity models show artifacts indicative of anisotropy with a characteristic north-south trend. Subsequent 2D anisotropic inversion images an anisotropic layer from 15 km to the Moho, with enhanced conductivity in the north-south direction. The extent of the anisotropic zone is wider than that of the Harrat, with its western edge aligned with a strand of the Najd fault system; the eastern edge lies beyond the study area. The anisotropic layer lies above a north-south trending zone of thinned lithosphere and a low-velocity zone in the underlying asthenosphere. It further coincides with the Makkah-Madinah-Nafud (MMN) line, a more than 600-km long alignment of volcanic vents with similar petrochemistry.

The observed electrical anisotropy is speculated to reflect a combination of deformation fabric and possibly aligned melt lenses within the lower crust. These may have developed in response to channeled asthenospheric flow transmitted through the mantle lid into the rheologically-weak lower crust. A zone of elevated mantle conductivity is shallowest beneath the Harrat, consistent with a lithospheric thickness of 60-80 km.

Keywords: anisotropy, magnetotelluric, Saudi Arabia, Harrat Rahat